Bars in Cuspy Dark Halos

John Dubinski[1], Ingo Berentzen[2] and Isaac Shlosman[3,4]

[1]Department of Astronomy and Astrophysics, University of Toronto,
50 St. George Street, Toronto, ON M5S 3H4, Canada
email: dubinski@astro.utoronto.ca

[2]Astronomisches Rechen-Institut,
Mönchhofstr. 12-14 69120, Heidelberg, Germany
email: iberent@ari.uni-heidelberg.de

[3]JILA, University of Colorado, Boulder, CO 80309-0440, USA; and

[4]Department of Physics and Astronomy, University of Kentucky,
Lexington, KY 40506-0055, USA
email: shlosman@pa.uky.edu

Abstract. We examine the bar instability in models with an exponential disk and a cuspy NFW-like dark matter (DM) halo inspired by cosmological simulations. Bar evolution is studied as a function of numerical resolution in a sequence of models spanning $10^4 - 10^8$ DM particles - including a multi-mass model with an effective resolution of 10^{10}. The goal is to find convergence in dynamical behaviour. We characterize the bar growth, the buckling instability, pattern speed decay through resonant transfer of angular momentum, and possible destruction of the DM halo cusp. Overall, most characteristics converge in behaviour for halos containing more than 10^7 particles in detail. Notably, the formation of the bar does not destroy the density cusp in this case. These higher resolution simulations clearly illustrate the importance of discrete resonances in transporting angular momentum from the bar to the halo.

Keywords. galaxies: spiral, structure, evolution; dark matter, methods: n-body simulations, stellar dynamics

1. Introduction

The bar instability in a cold gravitating disk plays a major role in a spiral galaxy's dynamical evolution. At least 2/3 of spiral galaxies host bars (Knappen *et al.* 2000) and the fraction has not evolved significantly since $z \sim 1$ (Jogee *et al.* 2004; Sheth *et al.* 2008). As models of galaxy formation become more sophisticated and reveal complex dynamical behaviour, it is important to understand the details of different physical processes that shape their morphology as well as to verify that numerical resolution is in fact adequate to follow their evolution. The bar-halo interaction is the driving mechanism in disk galaxy evolution. As a bar churns through the DM halo with a pattern speed Ω_b resonant interactions with halo orbits – a form of dynamical friction – transfer angular momentum from the bar to the halo and cause it to spin down (Tremaine & Weinberg 1984). This process was first pointed out by Lynden-Bell & Kalnajs (1972) and has been studied in models with idealized rigid bars (Weinberg 1985; Hernquist & Weinberg 1992; Weinberg & Katz 2002; Weinberg & Katz 2007) as well as in models in which a stellar bar forms self-consistently in an unstable disk (e.g., Sellwood 1980; Debattista & Sellwood 1998; O'Neill & Dubinski 2003; Holley-Bockelmann *et al.* 2005; Martinez-Valpuesta *et al.* 2006). There has been some concern that the process is too efficient,

leading to bars that are much smaller than their corotation radii and so discrepant with observed bar galaxies (Debattista & Sellwood 2000). More recent studies with greater resolution suggest that the bars tend to lengthen moving out to their co-rotation radii as they slow down and so perhaps they are not inconsistent with reality (O'Neill & Dubinski 2003; Martinez-Valpuesta *et al.* 2006). Weinberg & Katz (2002) hold a cautious view that lower resolution simulations can lead to spurious results because of the diffusive nature of noise that may move orbits into and out of resonances artificially while insufficient particle numbers may also underpopulate the resonant regions of phase space. While most current work to date has used $\sim 10^6$ particles, they claim that as many as 10^8 DM particles (or more) may be needed to simulate the resonant process with N-body methods.

In this study, we attempt to clear up the inconsistencies of current work and address the problem of numerical resolution hoping to converge to the correct physical behaviour. We present a series of bar-unstable disk+halo N-body models with increasing resolution spanning a range $N_h = 10^4 - 10^8$ DM particles with $N_d = 1.8 \times 10^{3-7}$ disk particles. One further simulation uses a multi-mass method that increases the halo particle number density by $200\times$ in the halo centre so giving an effective $N_h \sim 10^{10}$. The mass model is constructed from a 3-integral distribution function (Widrow & Dubinski 2005) describing an exponential disk embedded within a tidally truncated NFW halo and is similar to the model studied by Martinez-Valpuesta *et al.* (2006). Natural units for the simulations are $D = 10$ kpc, $M = 10^{11}$ M$_\odot$, $V = 208$ km/s, and $T = 47.2$ Myr. We discuss results both in simulation and physical units throughout and clarify when necessary. (For further details on the models and simulations see Dubinski, Berentzen & Shlosman 2008). Animations of the simulations are available for viewing at the URL: `www.cita.utoronto.ca/~dubinski/IAU254` along with higher-resolution figures.

Animation 1 shows the evolution of the disks in six models with increasing resolution in face-on and edge-on views. The lowest resolution simulations with $N_h \leqslant 10^5$ are clearly deficient and either lose the bar or suffer from heating affects. At higher resolution, the behaviour is similar exhibiting the buckling instability and relaxation to a bar in quasi-equilibrium that gradually lengthens and slows down. Animations 2 & 3 show the multi-mass model with $N_h = 10^8$ in an inertial and corotating frame and illustrate how the bar grows from noise from the inside out saturating as a thin bar on reaching the corotation radius and then evolving into a fatter bar with a peanut-shaped bulge after the buckling instability.

2. Bar Growth and Pattern Speed Evolution

We study bar growth using the normalized Fourier amplitude $|A_2|$ of the $m = 2$ disturbance in the plane of the disk within a fixed radius $R < 0.5$ (5 kpc). Figure 1 shown the exponential growth of $|A_2|$ before saturation. Higher resolution simulations reach saturation at later times. This time delay is the result of the lower amplitude of the Poisson fluctuations that seed the bar. Since the instability grows from these fluctuations if takes longer for them to saturate if the initial amplitude is lower. We estimate the time delays from the peak in $|A_2|$ and synchronize the simulations for comparison of various evolutionary characteristics.

We can also use A_2 to measure the phase angle of the $m = 2$ mode and so estimate the pattern speed by taking the difference between subsequent snapshots. Figure 2 shows the pattern speed evolution as a function of numerical resolution. There is some scatter in behaviour that can be accounted for from the expected variance introduced by different initial conditions but overall the agreement is good. The highest resolution simulations
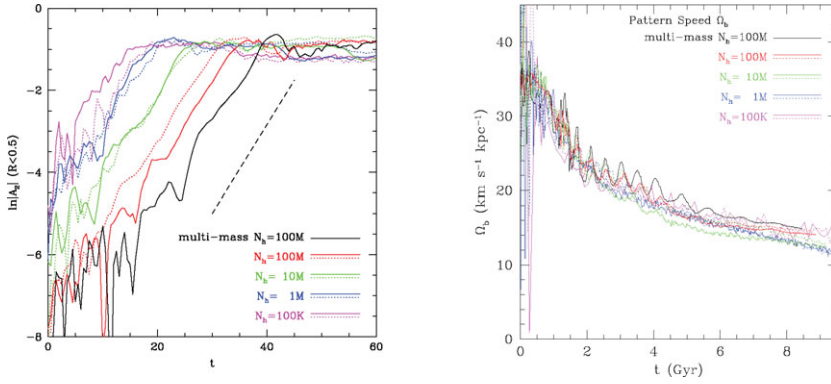
Figure 1. Initial growth of the $m = 2$ Fourier component $|A_2|$ for stars with $R < 0.5$ for two model sequences using $N_d = 18K, 180K, 1.8M, 18M$ with $N_h = 100K, 1M, 10M, 100M$ respectively. The $\ln|A_2|$ grows approximately linearly with time independent of the choice of N_d and N_h showing the exponential growth of the bar mode. The dashed line shows an exponential timescale that is approximately $\tau = 8$ (370 Myr). Since the bar grows from the Poisson noise within the disk then we expect the noise amplitude to be proportional to $N^{1/2}$ so larger simulations will saturate at later times.
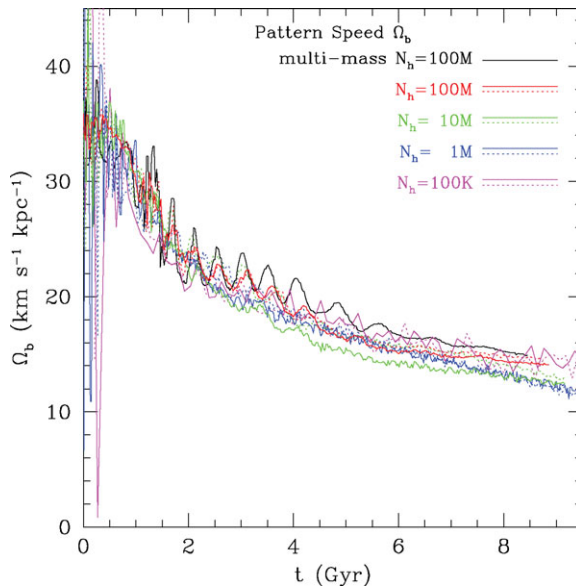

Figure 2. Evolution of the pattern speed Ω_b for two model sequences at different resolution. The curves have been shifted in time so that the bar growth evolution is coincident with the 1M particle model.

show a modulation of the pattern speed at a frequency close to Ω_b itself. This probably indicates an interaction between the bar and the gravitational wake in the halo that only shows up with sufficient numerical resolution.

3. Halo Density Profile

We also measured the evolution of the halo density profile over the course of the simulation. Previous work has shown both preservation and destruction of the density
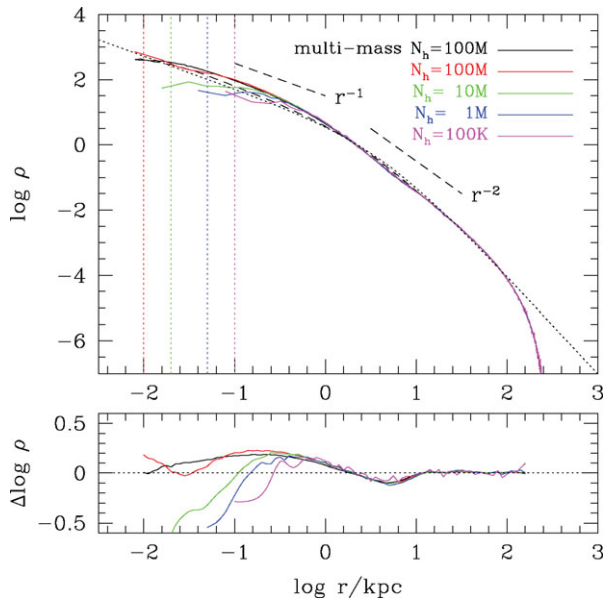
Figure 3. A comparison of density profiles at $t = 7.08$ Gyr for different halo particle numbers N_h. We also show the initial density profile (dashed line) and the best fit NFW model curve (dotted line) to the initial profile over the range $0 < r < 100$ kpc. The NFW parameters for the fit are $r_s = 4.3$ kpc, $v_{max} = 160$ km s^{-1}, where v_{max} is the maximum circular velocity at $r = 2.16 r_s = 9.3$ kpc. Note that this halo is more concentrated than the typical galactic dark matter halos in cosmological simulations to model the contraction expected during dissipative galaxy formation. The dotted vertical lines show the softening length ϵ used at different resolutions.

cusp so we focus on the processes in the central regions. Only studies using the self-consistent field N-body method (SCF) lead to a core (Holley-Bockelmann *et al.* 2005; Weinberg & Katz 2007b) and there has been some concern about numerical instabilities that arise in those methods (Selwood 2003). Figure 3 exhibits the final density profile along with the difference from the initial profile as a function of halo particle number. The profiles agree well to within the limit of their gravitational softening radius and show convergent behaviour. The cusp is not destroyed in this case but rather the central density increases modestly, by a factor of 2, as a result of the bar evolution, following its buckling, which leads to an increase in the central stellar density (Sellwood 2003).

The bar that forms in this simulation has a similar mass ratio $M_b/M_{halo} \approx 0.6$ but is much thicker than the fiducial rigid bar simulation in Weinberg *et al.* (2007b) that destroys the cusp. Their study also included thick bars which did not destroy the cusps and the bar that forms here overlaps with those in their study. We conclude that there is no direct contradiction with the most recent results of Weinberg *et al.* (2007b) but would argue that the thicker bar models are probably more relevant to real galaxies. Thin bars do not persist for long before responding to the buckling instability and so the rigid bar approximation is not applicable over a Hubble time and probably not relevant to most galaxies (Martinez-Valpuesta & Shlosman 2004).

4. Orbital Resonances

The bar slowdown is the result of dynamical friction that leads to angular momentum transport to the DM halo. The process is due to resonant interactions between the

rotating bar's pattern speed and the halo particles' azimuthal and radial orbital frequencies. When $l_1\Omega_r + l_2\Omega_\phi = m\Omega_b$ then orbital resonances occur and halo particles torque or are torqued by the bar leading to a change in angular momentum. We can estimate the orbital frequencies at a specific time by freezing the potential and integrating the orbits of particles in this potential rotating with the pattern speed at that time (e.g., Athanassoula 2002; Martinez-Valpuesta *et al.* 2006). Spectral analysis can then be applied to the orbital time series to determine the fundamental orbital frequencies Ω_r and Ω_ϕ (Binney & Spergel 1982). (Note we label these frequencies with the usual epicyclic variables $\kappa \equiv \Omega_r$ and $\Omega \equiv \Omega_\phi$ in our figures below.) The dimensionless frequency $\eta = (\Omega - \Omega_b)/\kappa$ is a useful way to characterize resonances since the values $\eta = 1/2, 0, -1/2$ correspond to the inner Lindblad, corotation, and outer Lindblad resonances for $m = 2$. Further negative half-integer values correspond to higher order resonances that can also absorb the angular momentum.
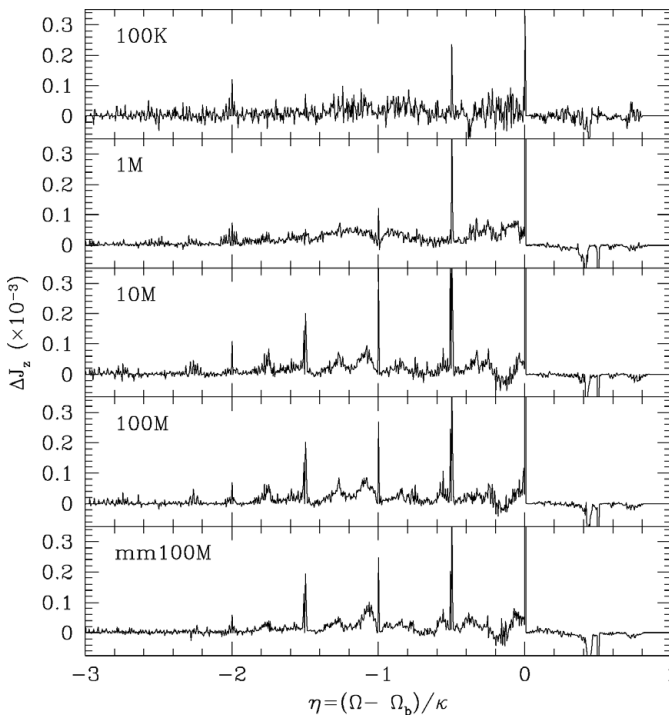

Figure 4. The distribution in the change in the z angular momentum ΔJ_z between $t = 100$ (4.7 Gyr) and $t = 150$ (7 Gyr) plotted as a function of the dimensionless frequency $\eta = (\Omega - \Omega_b)/\kappa$ measured at $t = 100$. The spikes at $\eta = 0.5, 0.0, -0.5$ correspond to the ILR, COR, and OLR respectively while other spikes refer to higher order resonances. This plot shows how halo particles in resonant orbits are the main sink of angular momentum. The detailed distributions are converging for $N_h > 10^7$ particles while lower resolution simulation miss some of the higher order resonances.

Figure 4 shows the change in the z component of the angular momentum J_z for particles binned as a function η between $t = 100$ and $t = 150$ at different numerical resolution. The spikes at the half-integer values reveal the resonances. Most angular momentum is transferred through the corotation resonance though it is also appears to be transferred at other frequencies, but more randomly – this difference is probably the result of particles in resonance before or after $t = 100$. The detailed behaviour of the distributions seem to
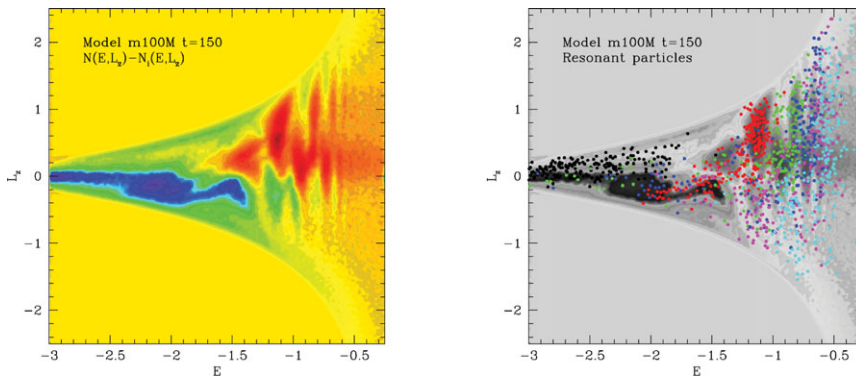
Figure 5. Change in particle number density in (E, L_z) space between $t = 0$ and $t = 150$ (7.0 Gyr) for the $N_h = 10^8$ single mass model. The resonant regions show up clearly as peaks (red regions) in phase space in the left panel. In the right panel, we overplot the (E, L_z) coordinates of a random subset of particles located at discrete resonances at $t = 150$ within $\delta\eta = \pm 0.05$ (black-ILR-$\eta = 0.5$, red-COR-$\eta = 0.0$, green-OLR-$\eta = -0.5$, blue-$\eta = -1.0$, magenta-$\eta = -1.5$, and cyan-$\eta = -2.0$.

converge for $N_h \geqslant 10^7$. At lower resolutions, the resonant spikes have a smaller amplitude and higher order resonant interactions are missing.

Finally, we examine the change in halo phase space density by computing the particle number density in (E, L_z) space and computing the difference between $t = 0$ and $t = 150$ in a similar way to Holley-Bockelmann *et al.* (2005). In this way, we clearly see the resonant regions visible as discrete islands of particle overdensity in (E, L_z) space (Fig. 5). We can also overplot the values of (E, L_z) for the particles found in the resonant spikes in the analysis to see where they lie in phase space. The right panel of Figure 5 clearly shows that these islands are directly related to the discrete resonances extracted in our spectral analysis. Animation 4 describes the time evolution of the differential number density in phase space and reveals how the resonances move through a large fraction of the halo mass. By counting particles in resonant peaks at different times we estimate that roughly 30% of the halo particles are affected.

We conclude that the resonances are broader than thought and so simulations with more than 1M halo particles do a reasonable job of tracking bar evolution. However, a look at the distribution of orbital frequencies reveals that higher order resonances are missed at lower resolution with less than 10M particles. This effect could account for the different rate of angular momentum loss at higher resolution. Future studies should examine the bar instability self-consistently using the same initial conditions with different N-body methods to resolve current inconsistent results on the cusp/core evolution of DM halos.

References

Athanassoula, E. 2002, *ApJ (Letters)*, 569, L83
Binney, J. & Spergel, D. 1982, *ApJ*, 252, 308
Debattista, V. P. & Sellwood, J. A. 1998, *ApJ (Letters)*, 493, L5+
—. 2000, *ApJ*, 543, 704
Dubinski, J. 1996, New Astronomy, 1, 133
Dubinski, J., Berentzen, I., & Shlosman, I. 2008, in prep.
Hernquist, L. & Weinberg, M. D. 1992, *ApJ*, 400, 80
Holley-Bockelmann, K., Weinberg, M., & Katz, N. 2005, *MNRAS*, 363, 991
Jogee, S., *et al.* 2004, *ApJ (Letters)*, 615, L105

Knapen, J. H., Shlosman, I., & Peletier, R. F. 2000, *ApJ*, 529, 93
Lynden-Bell, D. & Kalnajs, A. J. 1972, *MNRAS*, 157, 1
Martinez-Valpuesta, I. & Shlosman, I. 2004, *ApJ (Letters)*, 613, L29
Martinez-Valpuesta, I., Shlosman, I., & Heller, C. 2006, *ApJ*, 637, 214
O'Neill, J. K. & Dubinski, J. 2003, *MNRAS*, 346, 251
Sellwood, J. A. 1980, *A&A*, 89, 296
—. 2003, *ApJ*, 587, 638
Sheth, K. *et al.* 2008, *ApJ*, 675, 1141
Tremaine, S. & Weinberg, M. D. 1984, *MNRAS*, 209, 729
Weinberg, M. D. 1985, *MNRAS*, 213, 451
Weinberg, M. D. & Katz, N. 2002, *ApJ*, 580, 627
—. 2007a, *MNRAS*, 375, 425
—. 2007b, *MNRAS*, 375, 460
Widrow, L. M. & Dubinski, J. 2005, *ApJ*, 631, 838

John Dubinski explaining a fine point in his simulations.

Beatriz Barbuy illustrating the view of the Bulge through Baade's window.

Olga Sil'chenko fielding a question after her talk, with chairman Burkhard Fuchs.